



HAL
open science

THz-Based monitoring of the deformation of the inner woven structure of glass fiber reinforced polymers

Pascal Pomarède, Jaume Calvo-de la Rosa, Piotr Antonik, Fodil Meraghni, David S. Citrin, Damien Rontani, Alexandre Locquet

► **To cite this version:**

Pascal Pomarède, Jaume Calvo-de la Rosa, Piotr Antonik, Fodil Meraghni, David S. Citrin, et al.. THz-Based monitoring of the deformation of the inner woven structure of glass fiber reinforced polymers. IEEE Transactions on Terahertz Science and Technology, 2023, 13 (4), pp.396-404. 10.1109/TTHZ.2023.3275278 . hal-04273348

HAL Id: hal-04273348

<https://hal.science/hal-04273348>

Submitted on 7 Nov 2023

HAL is a multi-disciplinary open access archive for the deposit and dissemination of scientific research documents, whether they are published or not. The documents may come from teaching and research institutions in France or abroad, or from public or private research centers.

L'archive ouverte pluridisciplinaire **HAL**, est destinée au dépôt et à la diffusion de documents scientifiques de niveau recherche, publiés ou non, émanant des établissements d'enseignement et de recherche français ou étrangers, des laboratoires publics ou privés.

THz-BASED MONITORING OF THE DEFORMATION OF THE INNER WOVEN STRUCTURE OF GLASS FIBER REINFORCED POLYMERS

Authors

P. Pomarède^{1,2}, J. Calvo-de la Rosa^{1,3,4}, P. Antonik³, F. Meraghni², D.S. Citrin^{1,5}, D. Rontani³, and A. Locquet^{1,5}

Abstract—This work exploits terahertz (THz) imaging in the real-space and the spatial-frequency domain to determine nondestructively the evolution of the main characteristics of a woven glass-fiber reinforced polymer (GFRP) laminate in three-dimensions in-situ during a tensile test. These characteristics include tow orientation and the weave period. The surface and the inner plies can be investigated with the proposed method. The results show how the tows tend to realign with the load direction. In addition, we detect a decrease in the weave period, manifesting a distortion of the surface and inner layers as the stress is increased. Contrary to conventional optical inspection, THz inspection can provide quantitative measurements in all material layers and not only on the surface. This technique could be helpful to monitor distortion and damage due to mechanical stress or defects incorporated during the manufacturing process and to validate parameters and results of draping process modeling, especially for the inner plies.

KEYWORDS--Terahertz (THz), Tensile test, Non-Destructive Evaluation (NDE), GFRP

I. INTRODUCTION

Fiber-reinforced polymer composites are commonly employed as structural materials in applications requiring lightweight properties. The individual properties of the polymeric phase and the fiber reinforcements, as well as the way their spatial distribution, determine the mechanical performance of the composite [1–3]. More specifically, due to their remarkable mechanical properties, multi-ply composites with woven fabrics are currently employed in high-demand applications, such as aerospace [4–8]. Stresses suffered in service can damage these materials, reducing their performance and adversely impacting safety. In addition, tow orientation in the inner plies might

also be distorted during the manufacturing process in complex shaped structure [9,10]. It could induce unexpected local stress concentration which will lower the lifetime of the component. Therefore, it is common practice to perform routine inspection with the aim of detecting incipient fracture or other failure and validating results from draping process modeling.

The nondestructive evaluation (NDE) of fiber-reinforced composites is a field in continuous development due to its high technological importance for the early detection of defects. Terahertz (THz) imaging is gaining interest as a technology for NDE of a wide range of materials, and in particular for fiber-reinforced polymers such as glass-fiber (GFRP) and carbon-fiber (CFRP) reinforced polymers. Compared to other currently employed techniques, such as ultrasound [11–15] and X-ray tomography [16], THz NDE combines good transverse resolution (in the hundreds of μm) with the absence of ionizing radiation (thus safe to use). THz technology has already been used for detecting damage in composite materials – most often delamination – induced by tensile stress or impact tests, for instance in [17–21]. THz techniques have also been applied to evaluate fatigue-induced damage [22], heat damage [23,24], and laser shock [25], after manufacturing [26] or to evaluate the moisture content [27]. In addition to damage observation, THz is a promising technique to measure the matrix characteristics in the composite and the relative orientation of the fiber tows. Indeed, it has been shown that adding other plastics in a base resin during the compounding process can be evaluated from the THz refractive index [28–30]. Other works have shown that the THz absorption coefficient and refractive index can be used to characterize the plastic matrix of a composite [31]. Concerning the relative orientation of the tows, good results have already been achieved for unidirectionally oriented composites [32–37], while it is more challenging

Affiliations

1: Georgia Tech-CNRS IRL2958
Georgia Tech Lorraine, 2 Rue Marconi, 57070 Metz, France
e-mail: ppomarede@georgiatech-metz.fr, alocquet@georgiatech-metz.fr, david.citrin@ece.gatech.edu

2: Arts et Métiers Institute of Technology, CNRS, Université de Lorraine, LEM3-UMR 7239 CNRS
4 rue Augustin Fresnel, 57078 Metz, France
e-mail: fodil.meraghni@ensam.eu

3: LMOPS EA 4423 Laboratory, Chair in Photonics

CentraleSupélec & Université de Lorraine, 2 rue Edouard, Belin, F-57070, Metz, France
e-mail: piotr.antonik@centralesupelec.fr, damien.rontani@centralesupelec.fr

4: Department of Condensed Matter Physics, Faculty of Physics, Universitat de Barcelona, Martí i Franquès 1 08028 Barcelona, Spain
e-mail: jaumecalvo@ub.edu

5: School of Electrical and Computer Engineering, Georgia Institute of Technology, Atlanta, GA, 30332-0250, USA
e-mail: alocquet@georgiatech-metz.fr, david.citrin@ece.gatech.edu

in woven composites, where the fiber tows are present in multiple directions and due to the weave pattern are not purely planar. A recent contribution to the evaluation of the weave structure of a woven composites with THz has been made in [38], where the authors use the change in the transmittance spectrum when the polarization direction is parallel to the warp or the weft direction.

In this work, we use a recently reported THz-based image processing approach proposed by our team [39] to account for the fabric’s distortion during a tensile test in samples of thermoplastic-based GFRP reinforced by woven glass fibers. The approach hinges on analyzing the two-dimensional fast-Fourier transform (2D-FFT) modulus-squared pattern to extract the tow orientations and weave periods and is inspired by Refs. [40–42] on image analysis. It is known that off-axis tensile tests on woven composites will induce a significant reorientation of the fibers along the loading direction, distorting the fabric pattern [43,44]. This induced distortion affects the weave period, which, with the tow orientations [7,45,46], determines in part the mechanical properties of the composite [47–49]. Also, the shear properties of a woven structure are typically estimated by performing bias-extension tests (*i.e.*, tensile tests with the woven structure oriented 45° – 45°) [44,50,51]. Therefore, monitoring tow orientation and weave period would also enable one, in real-time, to assess the mechanical properties of the composite. By our proposed method, we can track the orientation of the warp and weft bundles, and the weave period, as a function of the applied load. We show that this monitoring can be performed on the woven structure in the surface layers as well as on the fabric in inner plies. The distortion of the initial weave structure can be understood as a measure of the damage caused to the composite. This approach, perhaps supplemented by visual inspection, may provide an adequate understanding of the material’s behavior in service.

In this paper, after introducing the material under study, preliminary tensile experiments are detailed to validate the parameters of the *in-situ* tensile tests in the THz scanner. Then, we present the results of the proposed THz-based image processing approach, for monitoring the structure of the woven fabric in the surface plies. Comparison is performed with measurements based on photographic images and with the analytic kinematic relation of the bias-extension, which links the in-plane shear angle to the extension of the sample. Finally, we demonstrate the capability of the proposed procedure to measure the state of the inner plies. In short, for the first time, we use THz imaging together with spatial Fourier transform of the images to detect in a nondestructive fashion stress-induced distortion of the weave pattern in GFRP laminates, not only in the surface plies, but also for inner plies.

II. EXPERIMENTAL CONDITIONS AND SETUP

Materials studied and preliminary experiments

The samples under investigation are polyamide 6 reinforced by 4 plies of 2/2 twill woven glass fibers manufactured by BÜFA (Oldenburg, Germany). All five rectangular samples considered in this paper are oriented at $\pm 45^\circ$ to the sides of the rectangular samples. The yarns oriented at 45° will be referred to as the warp and the ones oriented at -45° as the weft. The samples have been cut to a dimension of 117.5 x 30 x 2 mm³. Preliminary tensile tests have been carried out on two samples to measure the mechanical properties. A Z50 tensile test machine from the Zwick Roell group (Ulm, Germany) was used. We measure the strain using an extensometer from Epsilon Technology Corp (Jackson, Wyoming, USA), Model: 3542-025 M-010-ST) that clips on the sample to have a reliable measurement of the displacement. However, as the sample deformation before the breakage is large, we can only consider a maximal applied loading of 80 MPa when the contact extensometer is used to avoid damaging the latter. With this set-up, we extracted the Young modulus. Another experiment we carried out (without the contact extensometer) is to place the sample under tensile strain until sample breakage to obtain the stress to failure. The extracted mechanical properties of this composite are given in Table 1.

Young modulus (GPa)	Stress to failure (MPa)
7.7	180

Table 1: Measured mechanical properties of the polyamide 6/woven glass fibers with the tows oriented at $\pm 45^\circ$

We placed the samples in a tensile test stage from Miromecha (Metz, France, Model: Aquilax Max) for the *in-situ* THz scan. It has a force limit of 10 kN and a displacement resolution of 20 nm. After placing the sample in the stage, an area of 37 x 60 mm² only can be scanned due to geometrical constraints. We know that during a tensile test on a woven structure oriented $\pm 45^\circ$, with its initial length twice as long as its width, its deformed state can be divided in three zones A, B, and C (*see* Figure 1) [44,50,51]. As both ends of the specimen are clamped, there is no deformation in zone A. In zone C, both warp and weft have their ends free, leading to a constant pure shear deformation in this zone. Finally, in zone B, only one yarn direction is free, the other is being clamped, leading to a shear deformation of half the value of the one in zone C. Thus, in order to properly measure the variation of the yarn orientation, images have to be taken in zone C. It should be added that as the tensile stage applies a tension-tension loading, the center of the sample will remain fixed. Consequently, the THz scan can always be performed in zone C while keeping the same scanning parameters.

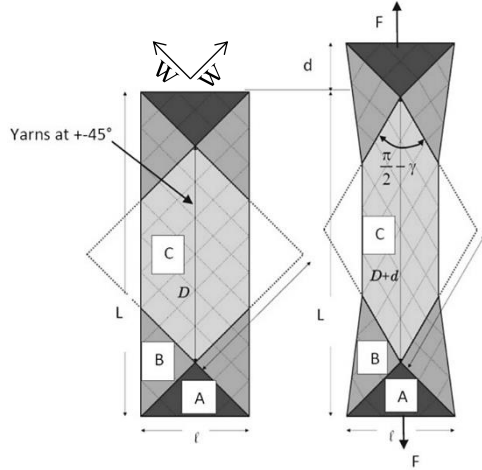


Figure 1: Woven fabric before (left) and after (right) a bias-extension test. The sample is clamped top and bottom. No deformation in zone A. In zone C, the two yarn directions have free ends leading to pure shear deformation. In zone B, one yarn direction has free ends leading to a shear deformation of half the value of zone C [44]

It is known that the polyamide 6 matrix experiences time dependent strain increase while maintaining a force due to its viscous properties [52,53]. In addition, the *in-situ* THz scans can take several tens of minutes to hours, depending on the spatial step size. To avoid artifacts in the THz-C scans, the sample displacement needs to remain small compared to the scan step size. We therefore perform a preliminary creep test to evaluate the magnitude of this deformation. This creep test is performed using the above-mentioned Z50 tensile test machine and extensometer. The sample is loaded until reaching 100 MPa, after which the load is maintained for 9000 s. Of note, since the extensometer could be damaged when measuring a deformation greater than 10 %, the extensometer was installed on the sample only after reaching the targeted 100 MPa (at $t=0$ on the Figure 2).

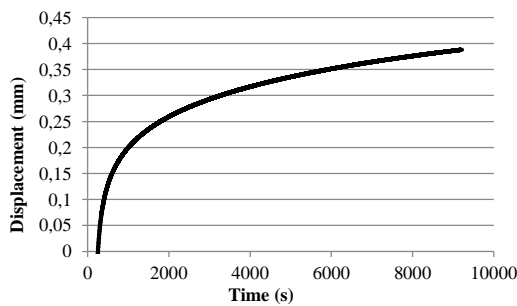


Figure 2: Displacement/time curve from a preliminary creep test performed on a polyamide 6/woven glass fibers with the fiber tows oriented at $\pm 45^\circ$ loaded at 100 MPa during 9000 s. The curve describes the displacement after 100 MPa is reached.

The results are shown in Figure 2. A large displacement is observed right after the load is applied, with total a of 0.38 mm for 9000 s of applied loading. However, a

displacement of only 0.080 mm occurs between $t = 3000$ s and $t = 9000$, so for 6000 s of applied loading. Consequently, for our *in-situ* measurements, we choose to wait for 5400 s before starting the THz scan to limit this creep displacement during the data acquisition. In addition, a step size of 0.5 mm was chosen since the duration for a $37 \times 60 \text{ mm}^2$ scan is about 5040 s. As we can expect a displacement of only 0.080 mm, it will not affect the results significantly.

THz C-Scan and signal processing

We analyze a total of five nominally identical samples using the same procedure. Each sample is placed in the tensile stage, and we perform a THz scan with a step size of 0.5 mm, for the x and y directions along a surface of $37 \times 60 \text{ mm}^2$. The samples are all scanned before applying any force in order to determine their initial structure. Then, we run a THz scan for every step of 20 MPa of applied stress (keeping the force constant during the scan) until reaching 140 MPa. Beyond this value the samples broke likely because of creep fatigue induced by the prior loading procedure that the samples undergo. This leads to a total of eight scans per sample.

We conduct a THz time-of-flight tomography (TOFT) experiment to stratigraphically map the samples at a room temperature of 22°C . These experiments were performed using a TeraView TPS Spectra 3000 (TeraView, Cambridge, UK). The sample surface is scanned pixel by pixel with a 0.5 mm step in both the x and y directions. At each pixel, a THz pulse is launched toward the sample, and the reflected signal is measured. Due to the refractive index mismatch between the air and the sample, and between the different components inside the sample which determine the Fresnel coefficients, we measure a set of time-delayed reflected pulses or *echoes* corresponding to different interfaces (*c.f.* Figure 3). This allows us to easily analyze the inner structure of the material by time-windowing the measured signals. The transverse resolution of the terahertz beam is $\sim 0.3 \text{ mm}$ at 1 THz, while its axial resolution is $\sim 46 \mu\text{m}$.

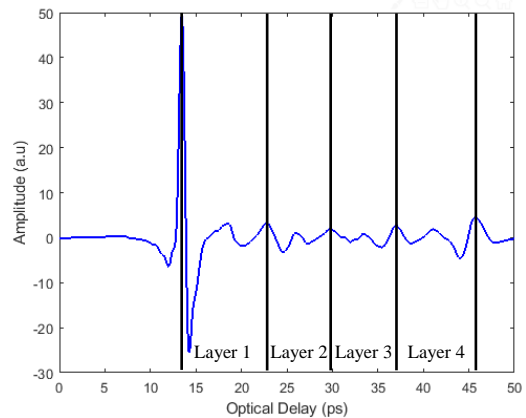


Figure 3: Typical THz time-domain waveform from a sample. Several echoes are visible, corresponding to the different interfaces. The locations of the four layers of the

sample are indicated on the figure. The vertical lines are added to indicate the interfaces between the plies.

The five different THz datasets are analyzed according to the methodology described below. First, we process the raw data by applying a bandpass filter with a frequency range from 0.2 THz to 1.5 THz. The resulting pulses were then filtered by wavelet denoising [54,55]. In this work, a symlet 4 wavelet was used, with a maximum level of 7, and the noise was removed by soft thresholding the least significant wavelet coefficients. The subsequent analyses are then performed on the 74 x 120 pixels C-scan data, performed at selected time slices, corresponding to the investigated layer of the sample. Figure 4 shows a representative surface C-scan. The initial perpendicular orientation of the fiber tows at $\pm 45^\circ$ from the vertical and horizontal axes can be observed in red on the C-scan. The two-dimensional fast Fourier transforms (2D-FFT) of the C-scans data are computed and filtered with a vertical and horizontal band-pass filter in order to isolate the information relate to the weave structure. The resulting 2D-FFT pattern allows the measurement of the tow orientation and of the weave period, for the warp and weft directions, at each of the different applied stresses. A schematic representation of these quantities is displayed in Figure 4.b. A more detailed explanation of this methodology can be found in [39].

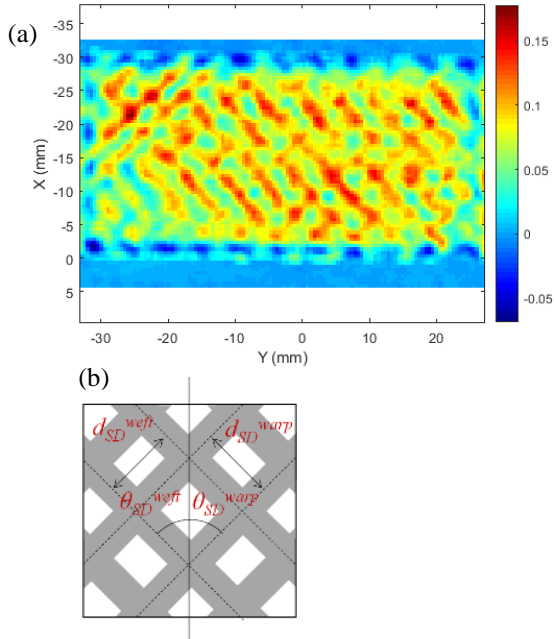


Figure 4. a: THz C-scan at the air-sample interface in Sample 1. The $\pm 45^\circ$ tow orientation is visible. b: Schematic representation of the weave period (d_{SD}) and angle (θ_{SD}).

An example of the 2D-FFT modulus-squared pattern obtained with the methodology mentioned is depicted, in Figure 5.a, for sample 1 with no stress applied. The four visible peaks in the spectrum represents the periodicities observed in the C-scan, which reflect the weave. Due to the pattern symmetry, only its bottom part will be considered. Two sets of spatial-frequency coordinates, $[u_1, v_1] =$

$[-0.18 \text{ mm}^{-1}, 0.18 \text{ mm}^{-1}]$ and $[u_2, v_2] = [0.19 \text{ mm}^{-1}, 0.178 \text{ mm}^{-1}]$, are obtained. From this, the tow orientations and the yarns period can be calculated, giving respectively -45° and 4.0 mm for the warp and 46.9° and 4.0 mm for the weft direction and period.

To validate the THz-based approach just discussed, a comparison analysis including direct measurements from photographs is also performed. For this purpose, we took photos of the top surface of samples for various applied stresses using a 4000 x 2250 pixels digital camera to reach a 30 $\mu\text{m}/\text{pixel}$ resolution. The variation of the two tow orientations and the period, have been measured with ImageJ software. Several yarns in zone C from Figure 1 were measured and averaged for each applied stress. These measurements confirmed the aforementioned values obtained on sample 1. The other direct measurements will be presented in the following section

III. RESULTS AND DISCUSSION

We will now present the evolution of the tow orientation and weave period while increasing the applied stress measured *in situ* by THz experiments. Results were obtained for the samples' top surface and inner plies.

Tow orientation and weave period at the top surface

In Figure 5.b, we present the evolution of the orientation of the warp and weft with the applied stress on sample 1. The orientation angles tend to decrease when increasing the applied load, implying that the tows are preferentially re-aligned toward the loading direction. The orientation angle of the warp continues to reduce by 30 % from its initial value at 140 MPa. Of note, the orientation of the weft cannot be measured after 100 MPa due to the development of stress-induced surface damage, with cracks and fiber buckling (see Figure 6), as is typical for off-axis tensile stress applied to woven fiber composites [45].

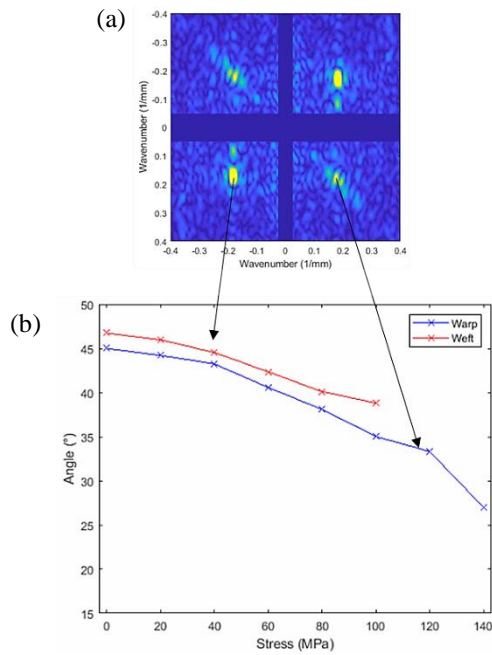


Figure 5: a: Results of the 2DFFT procedure on the sample 1 (no stress applied) with the two tow orientations detected. The two orientations $+45^\circ$ and -45° can be obtained. A mirror symmetry due to the 2DFFT is visible. b: Evolution of the two tow orientations with applied stress on sample 1. One of the orientations cannot be measured after 100MPa

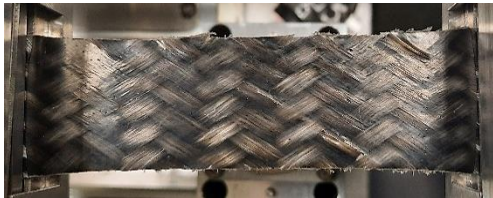


Figure 6: Photograph of top surface of one sample when reaching 140 MPa. Several cracks are visible inducing amplitude loss in the reflected THz signal.

In order to assess the width of the distribution of tow orientation, Figure 7.a shows the average and the standard deviation of the orientation over all five studied samples at each stress level. Again, we observe an overall decrease of the orientations with loading in these average values. The standard deviation across measurements is $\sim 4^\circ$ (8.9 %) for the warp and weft tows over all applied stress loading. The two tow orientations follow the same evolution with the applied stress consistent with the sample symmetry and loading. Of note, only one measurement has been obtained for the weft direction at 140 MPa, accounting for the zero value of the standard deviation appearing in the figure.

An important observation from these results is that fabrics in the unstressed, as-manufactured GFRPs studied are not ideal in that their orientation deviates slightly from the expected 45° . The technique employed here is able to reveal such deviations that, in turn, may affect the

mechanical and other properties [56]. In the sequel, to focus on stress-induced changes, the measured tow orientations are shifted in Figure 7.b, for each sample, to start at 45° when no stress is applied. The data averaged over all samples are shown in Figure 7.b with the new computed standard deviation. We notice an apparent overall decrease in the latter. Indeed, the range of the standard deviation now remains around 1° (2.2 %). This confirms that the distortion of the weave structure during the *in-situ* tensile test exhibits the same trend over the five investigated samples.

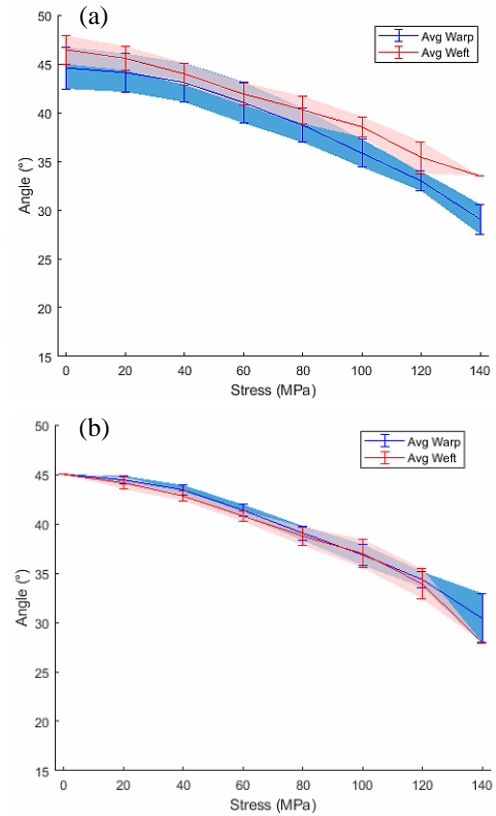


Figure 7. a: Variation of tow orientations (warp: blue, weft: red) as functions of stress obtained from surface THz data. The mean (central curve within the respective band) has been calculated over 5 samples; bands indicate one standard deviation from the mean. b: Variation of tow orientations as functions of stress with the values shifted in order to have all the orientations at 45° at 0 MPa. Both figures show a clear decrease of the orientation angle indicating the distortion of the weave pattern induced by the applied loading.

Figure 8.a (warp) and Figure 8.b (weft) shows the tow orientations on the sample surface obtained with direct measurements from sample photographs. Good agreement between the THz and visual data is observed.

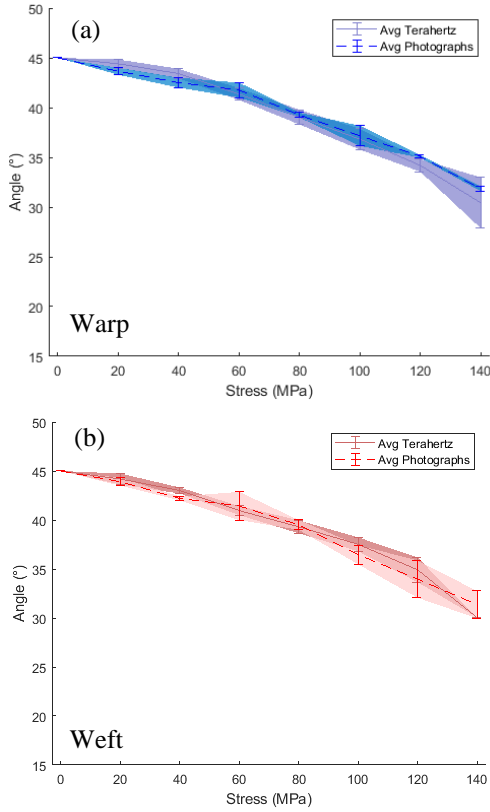


Figure 8: Variation of tow orientations (a) warp and (b) weft as functions of stress, with the values for each sample shifted to 45° at 0 MPa, obtained from surface THz data compared with photographs. The mean (central curve within the respective band) has been calculated over 5 samples; bands indicate one standard deviation from the mean. Good agreement between THz and visual data is observed.

Additionally, we measure the change in the weave period for each applied stress level. As for the tow orientation, all five samples are analyzed with the mean and standard deviation shown in Figure 9.a and b, for respectively the warp and weft. The standard deviation is about 0.14 mm (3.6 %) for the warp and 0.1 mm (2.6 %) for the weft. We observe a decrease of the weave period in both the warp and weft for stress > 60 MPa. Indeed, when the applied stress is lower there is only rotations field taking place inside a yarn [44], so no change yet in the weave period. In addition, the polyamide matrix acts to reduce the tows motions but only succeed before 60 MPa of applied stress. The tows begin then to move closer with each other as with a weave fabric alone. The necking of the sample increase even more this variation in the weave period. The necking on the sample is represented in Figure 1.b and can be observed in Figure 6.

Comparison of the weave period obtained from THz measurements with those from photographs is shown in Figure 9.a and b. Both sets of fibers exhibit similar behavior for the two measurements methods; deviations

are observed, especially for the warp fibers, but remain in the range of the standard deviation.

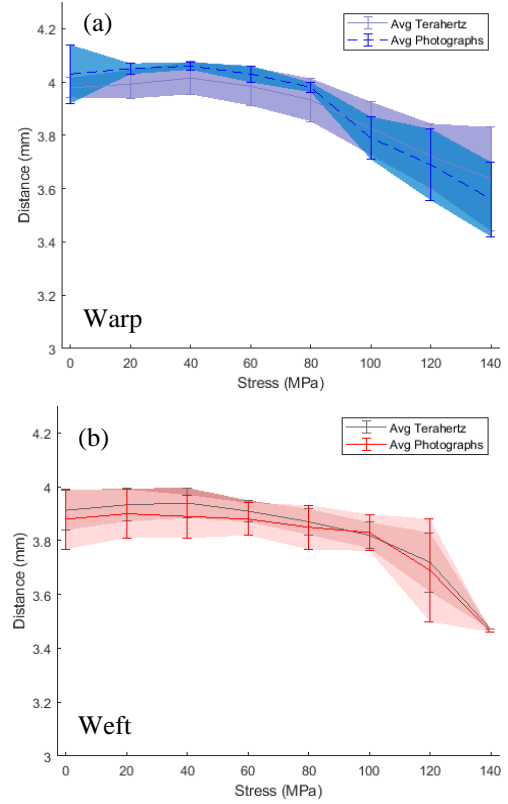


Figure 9: Variation of weave period for (a) warp and (b) weft as functions of stress obtained from surface THz data compared with photographs. The mean (central curve within the respective band) has been calculated over 5 samples; bands indicate one standard deviation from the mean. A clear decrease of the weave period after 60 MPa is noted, indicating a distortion in the fabric induced by the applied loading. Good agreement between THz and visual data is observed.

Comparison with theory

To further validate our proposed technique, we compare our observations with an analytic description, the kinematic relation of the bias-extension tests [44,50,51]. The kinematic relation of the bias-extension test links the shear γ with the applied displacement d on the sample by the tensile test machine

$$\gamma = \frac{\pi}{2} - 2\text{Arcos}\left(\frac{D+d}{\sqrt{2}D}\right) \mid D = L - l. \quad (\text{Eq.1})$$

The reader can refer to Figure 1 to see a representation of the bias-extension test and the quantities used in the equation. This relation is commonly applied to understand the CFRP behavior for the bias-extension test (tensile tests with the woven structure oriented 45°/-45°) and helps provide input data for the material drape model. This relation is valid under the following assumptions: (i) the yarns are inextensible during the test, (ii) no slippage between the weft and warp yarns (or no change in the

weave periodicity), and (iii) bending stiffness can be neglected.

In Figure 10, we show the average of the weft and warp orientations extracted from the THz data and the analytical kinematic relation. The applied displacement in this relation was obtained from tensile tests on the Z050 with an extensometer. As explained before, this tensile test can only reach 80 MPa.

Excellent agreement between theory and THz experiment is found until 80 MPa. It shows that the proposed technique provides results consistent with analytical expectations in this range. Beyond 80 MPa the discrepancy is tentatively assigned to slippage between the weft and warp yarns that initiates at ~ 60 MPa and becomes increasingly marked 80 MPa of applied loading. This means that one of the assumptions to use this analytical relation does not hold anymore when reaching this level of applied loading making the comparison irrelevant.

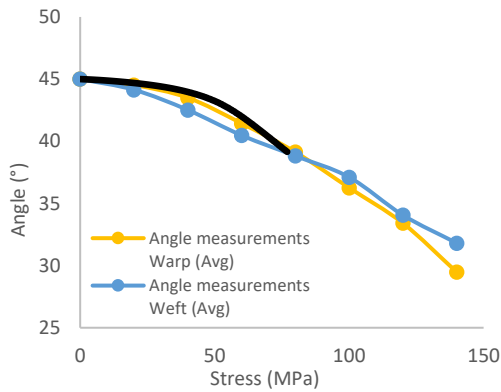


Figure 10: Comparison between THz results and the kinematic relation of the bias-extension test. The experimental average value of the warp and weft orientation with applied stress obtained from THz data (warp orange, weft blue) is shown together with the kinematic relation of the shear angle (black). Excellent agreement is obtained until 80MPa

Analysis of the inner structure

The discussion thus far has focused on the weave properties obtained from surface data. Evidently, the THz approach shows little utility from this perspective. The advantage of the THz probe relies on its ability to provide information about stress-induced changes to the weave pattern in inner plies, which the photographic evidence cannot. In this section, we study the evolution of the tow orientation in the inner plies of the composite material. To do so, we analyze C-scans at various time-delays corresponding to different depths. More specifically, we will consider the delay times $t = 22.67$, 34.47 , and 47.9 ps, corresponding to layers 2, 3, and 4 of the studied material. We first consider sample 5. As the signal penetrates deeper into the composite, it experiences significant attenuation,

as can be seen in Figure 3. A C-scan of sample 5 at $t = 22.67$ ps is shown in Figure 11.a. We observe that the image is noisier than in Figure 4, even though the warp and weft orientations are still visible. The noisier image results from the fact that as the signal penetrates deeper into the composite material, it experiences significant attenuation leading to strong attenuation of the amplitude of the signal (as seen in Figure 3). We have tested multiple filtering conditions and observed the repercussion it has on the weave pattern observation at the air-sample interface. This study demonstrated that a 0.3-0.4 THz band-pass filter (Figure 11.c) is the one that accentuates the most the weave structure, in which leads to the filtered C-scan shown in Figure 11.b. We first note that the echoes from the inner layers are still clearly visible as we can see on a typical A-scan, after applying the band-pass filter, depicted in Figure 11.d. Then, what is observed in Figure 11.a without filtering is the alternation between the yarns going up and down due to refractive-index mismatch between the matrix and the fibers, which corresponds to a large repetition period and have a high amplitude on the response spectrum (cf. Figure 11.c). By selecting the frequency range corresponding to the yarn dimensions, the $-45^\circ/45^\circ$ pattern, which has a lower repetition period and therefore associate to a smaller wavelength, can be more visible despite its lower amplitude.

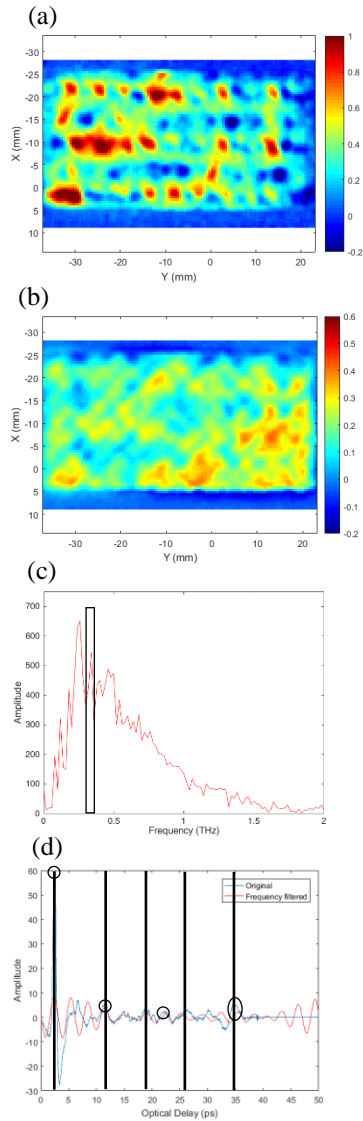


Figure 11: THz C-scan of sample 5 at $t = 22.67\text{ps}$ (a) before and (b) after applying a 0.3-0.4 THz bandpass filter. (c): Typical THz spectrum at one pixel on sample 5 with the 0.3-0.4 THz frequency band indicated in black. (d): Typical THz signal at one pixel on sample before and after applying the 0.3-0.4 THz bandpass filter.

The approach has been applied to all 5 studied samples to get an average evolution. As discussed above, the results for the various samples are shifted to 45° when no tensile stress is applied. The obtained averaged evolution is displayed in the Figure 12.a for the four layers (the values of t above) of the material considered. The result for the top surface (Layer 1) is included. We observe an evolution of the yarn orientation that is similar for the four layers, with a $\sim 30\%$ decrease of the angle at 140 MPa. In addition, the averaged curves for the 4 layers show a tendency to overlap. The low standard deviation observed demonstrates our experiments' reproducibility and the analysis' robustness.

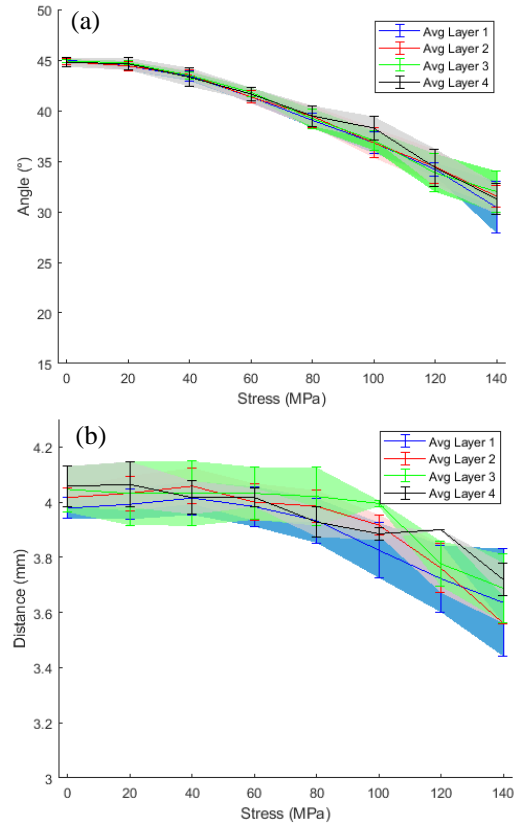


Figure 12:a: Variation of (a) yarn orientation (with value normalized to zero at 0 MPa) and (b) weave period for as functions of stress for four layers in the samples. The mean (central curve within the respective band) has been calculated over 5 samples; bands indicate one standard deviation from the mean. Only the weft direction is indicating for a better visibility. A clear decrease of the orientation angle indicates the stress-induced distortion of the weave pattern in various layers. Note that the fiber's orientations values have been shifted in order to have all the orientations at 45° at 0 MPa.

Finally, we show in Figure 12.b the evolution of the weave period (weft only for clarity) at time delays $t = 22.67$, 34.47, and 47.9 ps, corresponding to layers 2, 3, and 4. The top ply is also included and labelled Layer 1. We see that the decrease of the weave period occurs in all plies, not just the top. Little change is observed below 60 MPa, followed by a continuous decrease of the weave period, which is reduced by $\sim 10\%$ at 140 MPa.

The observed decrease of both the yarn orientation angles and the weave period indicates a distortion of the four fabric layers when loaded in tension. This result is of great potential interest as, contrary to other surface inspection techniques, the stress-induced deformation of the weave pattern can be monitored not only for the surface but also for the inner plies.

IV. CONCLUSIONS

In this paper, we have applied an experimental and image processing methodology to THz TOFT measurements, performed in reflection from one side of a woven-fiber polyamide 6 matrix GFRP laminate carried out *in situ* under tensile stress. We monitored the evolution of the warp/weft tow orientation and of the weave period with increasing tensile load.

By performing a Fourier analysis (2D-FFT) of the C-scan obtained for various time windows (associated with various depths in the samples), we detect the stress-induced deformation of the fabric, not only on the surface but for the first time in inner plies of the GFRP laminate. Moreover, the approach is contactless and non-destructive.

With our approach, one can observe a clear reorientation of the fiber structure along the loading direction in all four plies, consistent with analytical predictions. It is also possible to observe a decrease of the weave period in all four plies indicating a distortion of the fabric induced by the applied loading. While the results shown here are obtained under *in situ* stress, the approach can also be applied to cases where the stress has been applied and then released.

A major advantage of using THz TOFT presented here compared to surface-inspection techniques is the ability to image the impact of tensile load on the inner plies of the composite laminate. It provides a more global view of the deformation in the composite material and is essential as complex yarns deformation could occur inside the sample during shaping processes. This method could find applications in quality control in manufacturing or during maintenance inspection to ensure that the structure follows its designed specifications and to assess the effect of loading on the material. It could also be used to validate draping simulation model.

V. ACKNOWLEDGEMENTS

A.L., D.S.C, J.C.d.I.R., D.R. and P.A. acknowledge the financial support of the Région Grand Est. A.L and D.S.C. thank the CPER SusChemProc. A.L, D.S.C., P.P, and F.M acknowledge financial support from Institut Carnot ARTS. D.R and P.A. acknowledge the support of the Chair in Photonics.

VI. REFERENCES

[1] Ishikawa T, Chou TW. Elastic Behavior of Woven Hybrid Composites: J Compos Mater 1982;16:2–19. <https://doi.org/10.1177/002199838201600101>.

[2] Lomov S V., Huysmans G, Luo Y, Parnas RS, Prodromou A, Verpoest I, et al. Textile

composites: modelling strategies. Compos Part A Appl Sci Manuf 2001;32:1379–94. [https://doi.org/10.1016/S1359-835X\(01\)00038-0](https://doi.org/10.1016/S1359-835X(01)00038-0).

[3] Gay D. Matériaux composites . 6th editions. Lavoisier; 2015.

[4] Soutis C. Fibre reinforced composites in aircraft construction 2005;41:143–51. <https://doi.org/10.1016/j.paerosci.2005.02.004>.

[5] Ospald F, Zouathi W, Beigang R, Matheis C, Recur B, Guillet J, et al. Aeronautics composite material inspection with a terahertz time-domain spectroscopy system 2014;0–14.

[6] Wang Q, Li X, Chang T, Zhang J, Liu L, Zhou H, et al. Nondestructive imaging of hidden defects in aircraft sandwich composites using terahertz time-domain spectroscopy. Infrared Phys Technol 2019;97:326–40. <https://doi.org/10.1016/j.infrared.2019.01.013>.

[7] Cox BN, Flanagan G. Handbook Composites of Analytical Methods for Textile. 1997.

[8] Neale G, Dahale M, Yoo S, Toso N, McGarrigle C, Quinn J, et al. Improved crush energy absorption in 3D woven composites by pick density modification. Compos Part B Eng 2020;192:108007. <https://doi.org/10.1016/J.COMPOSITESB.2020.108007>.

[9] Kim DJ, Yu MH, Lim J, Nam B, Kim HS. Prediction of the mechanical behavior of fiber-reinforced composite structure considering its shear angle distribution generated during thermo-compression molding process. Compos Struct 2019;220:441–50. <https://doi.org/10.1016/j.compstruct.2019.04.043>.

[10] Kang H, Shan Z, Zang Y, Liu F. Effect of Yarn Distortion on the Mechanical Properties of Fiber-Bar Composites Reinforced by Three-Dimensional Weaving. Appl Compos Mater 2016;23:119–38. <https://doi.org/10.1007/s10443-015-9452-5>.

[11] Eckel S, Meraghni F, Pomarède P, Declercq NF. Investigation of Damage in Composites Using Nondestructive Nonlinear Acoustic Spectroscopy. Exp Mech 2017;57. <https://doi.org/10.1007/s11340-016-0222-6>.

[12] Castellano A, Fraddosio A, Piccioni MD. Quantitative analysis of QSI and LVI damage in GFRP unidirectional composite laminates by a new ultrasonic approach. Compos Part B Eng 2018;151:106–17. <https://doi.org/10.1016/j.compositesb.2018.06.003>.

[13] Smith RA, Clarke B. Ultrasonic C-scan determination of ply stacking sequence in carbon-fibre composites. Insight 1994;36:741–7.

- [14] Ibrahim ME. Ultrasonic inspection of hybrid polymer matrix composites. *Compos Sci Technol* 2021;208:108755. <https://doi.org/10.1016/j.compscitech.2021.108755>.
- [15] Li C, Pain D, Wilcox P, Drinkwater B. Imaging composite material using ultrasonic arrays. *AIP Conf Proc* 2012;1430.
- [16] Pomarède P, Meraghni F, Peltier L, Delalande S, Declercq NF. Damage Evaluation in Woven Glass Reinforced Polyamide 6.6 Composites Using Ultrasound Phase-Shift Analysis and X-ray Tomography. *J Nondestruct Eval* 2018;37. <https://doi.org/10.1007/s10921-018-0467-3>.
- [17] Lam PM, Lau KT, Ling HY, Su Z, Tam HY. Acousto-ultrasonic sensing for delaminated GFRP composites using an embedded FBG sensor. *Opt Lasers Eng* 2009;47:1049–55. <https://doi.org/10.1016/j.optlaseng.2009.01.010>.
- [18] Dong J, Pomarède P, Chehami L, Locquet A, Meraghni F, Declercq NF, et al. Visualization of subsurface damage in woven carbon fiber-reinforced composites using polarization-sensitive terahertz imaging. *NDT E Int* 2018;99:72–9. <https://doi.org/10.1016/j.ndteint.2018.07.001>.
- [19] Dong J, Locquet A, Declercq NF, Citrin DS. Polarization-resolved terahertz imaging of intra- and inter-laminar damages in hybrid fiber-reinforced composite laminate subject to low-velocity impact. *Compos Part B Eng* 2016;92:167–74. <https://doi.org/10.1016/j.compositesb.2016.02.016>.
- [20] Han DH, Kang LH. Nondestructive evaluation of GFRP composite including multi-delamination using THz spectroscopy and imaging. *Compos Struct* 2018;185:161–75. <https://doi.org/10.1016/j.compstruct.2017.11.012>.
- [21] Xu Y, Hao H, Citrin DS, Wang X, Zhang L, Chen X. Three-dimensional nondestructive characterization of delamination in GFRP by terahertz time-of-flight tomography with sparse Bayesian learning-based spectrum-graph integration strategy. *Compos Part B Eng* 2021;225:109285. <https://doi.org/10.1016/J.COMPOSITESB.2021.109285>.
- [22] Lopato P, Chady T. Terahertz examination of fatigue loaded composite materials. *Int J Appl Electromagn Mech* 2014;45:613–9. <https://doi.org/10.3233/JAE-141884>.
- [23] Hsu DK, Im KH, Chiou CP, Barnard DJ. An exploration of the utilities of terahertz waves for the NDE of composites. *AIP Conf Proc* 2011;1335:533–40. <https://doi.org/10.1063/1.3591897>.
- [24] Radziński M, Mieloszyk M, Rahani EK, Kundu T, Ostachowicz W. Heat induced damage detection in composite materials by terahertz radiation. <https://doi.org/10.1117/12.2084144>. <https://doi.org/10.1117/12.2084144>.
- [25] Malinowski PH, Ostachowicz WM, Touchard F, Boustie M, Chocinski-Arnault L, Gonzalez PP, et al. Study of plant fibre composites with damage induced by laser and mechanical impacts. *Compos Part B Eng* 2018;152:209–19. <https://doi.org/10.1016/J.COMPOSITESB.2018.07.004>.
- [26] Yakovlev E V., Zaytsev KI, Dolganova IN, Yurchenko SO. Non-Destructive Evaluation of Polymer Composite Materials at the Manufacturing Stage Using Terahertz Pulsed Spectroscopy. *IEEE Trans Terahertz Sci Technol* 2015;5:810–6. <https://doi.org/10.1109/TTHZ.2015.2460671>.
- [27] Ibrahim ME, Headland D, Withayachumnankul W, Wang CH. Nondestructive Testing of Defects in Polymer–Matrix Composite Materials for Marine Applications Using Terahertz Waves. *J Nondestruct Eval* 2021;40. <https://doi.org/10.1007/S10921-021-00767-9>.
- [28] Wietzke S, Jansen C, Rutz F, Mittleman DM, Koch M. Determination of additive content in polymeric compounds with terahertz time-domain spectroscopy. *Polym Test* 2007;26:614–8. <https://doi.org/10.1016/J.POLYMERTESTING.2007.03.002>.
- [29] Krumbholz N, Hochrein T, Vieweg N, Hasek T, Kretschmer K, Bastian M, et al. Monitoring polymeric compounding processes inline with THz time-domain spectroscopy. *Polym Test* 2009;28:30–5. <https://doi.org/10.1016/J.POLYMERTESTING.2008.09.009>.
- [30] Yang Z, Wang Q, Cao Z, Wang X, Peng Y. Quantitative Analysis of Metal Particles Concentration in the Composites Based on Terahertz Linear Scatter Method. *IEEE Trans Terahertz Sci Technol* 2020;10:490–4. <https://doi.org/10.1109/TTHZ.2020.3001515>.
- [31] Naftaly M, Miles RE. Terahertz time-domain spectroscopy for material characterization. *Proc IEEE* 2007;95:1658–65. <https://doi.org/10.1109/JPROC.2007.898835>.
- [32] Jördens C, Scheller M, Wietzke S, Romeike D, Jansen C, Zentgraf T, et al. Terahertz spectroscopy to study the orientation of glass fibres in reinforced plastics. *Compos Sci Technol* 2010;70:472–7. <https://doi.org/10.1016/j.compscitech.2009.11.022>.
- [33] Albrecht K, Baur E, Endres HJ, Gente R, Graupner

- N, Koch M, et al. Measuring fibre orientation in sisal fibre-reinforced, injection moulded polypropylene – Pros and cons of the experimental methods to validate injection moulding simulation. *Compos Part A Appl Sci Manuf* n.d.;95:54–64. <https://doi.org/10.1016/j.compositesa.2016.12.022>.
- [34] Park DW, Oh GH, Kim HS. Predicting the stacking sequence of E-glass fiber reinforced polymer (GFRP) epoxy composite using terahertz time-domain spectroscopy (THz-TDS) system. *Compos Part B Eng* 2019;177:107385. <https://doi.org/10.1016/j.compositesb.2019.107385>.
- [35] Im KH, Hsu DK, Chiou CP, Barnard DJ, Yang IY, Park JW. Influence of terahertz waves on the fiber direction of CFRP composite laminates. *AIP Conf Proc* 2013;1511:604–11. <https://doi.org/10.1063/1.4789102>.
- [36] Pflieger M, Katletz S, Pühringer H, Focke O, Wiesauer K. Measurement of the glass fiber orientation of single and double layers by polarized THz radiation. *Int Conf Infrared, Millimeter, Terahertz Waves, IRMMW-THZ 2013*. <https://doi.org/10.1109/IRMMW-THZ.2013.6665637>.
- [37] Park JW, Im KH, Hsu DK, Jung JA, Yang IY. Terahertz spectroscopy approach of the fiber orientation influence on CFRP composite solid laminates. *J Mech Sci Technol* 2012;26:2051–4. <https://doi.org/10.1007/S12206-012-0513-5>.
- [38] Tang C, Tanabe T, Yodate S, Oyama Y. Quantitative evaluation of fiber structure by using coherent terahertz wave. *Compos Part B Eng* 2019;159:1–3. <https://doi.org/10.1016/J.COMPOSITESB.2018.08.135>.
- [39] Calvo-de la Rosa J, Pomarède P, Antonik P, Meraghni F, Citrin DS, Rontani D, et al. Determination of the process-induced microstructure of woven glass fabric reinforced polyamide 6.6/6 composite using terahertz pulsed imaging. *NDT E Int* 2023:102799. <https://doi.org/10.1016/j.ndteint.2023.102799>.
- [40] Escofet J, Millán MS, Ralló M. Modeling of woven fabric structures based on Fourier image analysis. *Appl Opt* 2001;40:6170. <https://doi.org/10.1364/ao.40.006170>.
- [41] Chan C-H, Pang GKH. Fabric defect detection by Fourier analysis. *IEEE Trans Ind Appl* 2000;36:1267–76.
- [42] Jeong YJ, Jang J. Applying image analysis to automatic inspection of fabric density for woven fabrics. *Fibers Polym* 2005;6:156–61. <https://doi.org/10.1007/BF02875608>.
- [43] Karayaka M, Kurath P. Deformation and Failure Behavior of Woven Composite Laminates. *J Eng Mater Technology* 1994;116:222–32.
- [44] Boisse P, Hamila N, Madeo A, Hivet G, Isola D. The bias-extension test for the analysis of in-plane shear properties of textile composite reinforcements and prepregs : a review. *Int J Mater Form* 2017;10.
- [45] Pandita SD, Huysmans G, Wevers M, Verpoest I. Tensile fatigue behaviour of glass plain-weave fabric composites in on- and off-axis directions. *Compos Part A Appl Sci Manuf* 2001;32:1533–9. [https://doi.org/10.1016/S1359-835X\(01\)00053-7](https://doi.org/10.1016/S1359-835X(01)00053-7).
- [46] Holmes J, Sommacal S, Das R, Stachurski Z, Compston P. Characterisation of off-axis tensile behaviour and mesoscale deformation of woven carbon-fibre/PEEK using digital image correlation and X-ray computed tomography. *Compos Part B Eng* 2022;229:109448. <https://doi.org/10.1016/J.COMPOSITESB.2021.109448>.
- [47] Dixit A, Mali HS, Misra RK. Unit Cell Model of Woven Fabric Textile Composite for Multiscale Analysis. *Procedia Eng* 2013;68:352–8. <https://doi.org/10.1016/J.PROENG.2013.12.191>.
- [48] Crookston JJ, Long AC, Jones IA. A summary review of mechanical properties prediction methods for textile reinforced polymer composites. *Proc Inst Mech Eng Part L J Mater Des Appl* 2005;219:91–109. <https://doi.org/10.1243/146442005X10319>.
- [49] Lee S-K, Byun J-H, Hyung Hong S. Effect of fiber geometry on the elastic constants of the plain woven fabric reinforced aluminum matrix composites. *Mater Sci Eng A* 2003;346–58.
- [50] Launay J, Hivet G, Duong A V., Boisse P. Experimental analysis of the influence of tensions on in plane shear behaviour of woven composite reinforcements. *Compos Sci Technol* 2007.
- [51] Lebrun G, Bureau MN, Denault J. Evaluation of bias-extension and picture-frame test methods for the measurement of intraply shear properties of PP/glass commingled fabrics. *Compos Struct* 2003;61:341–52. [https://doi.org/10.1016/S0263-8223\(03\)00057-6](https://doi.org/10.1016/S0263-8223(03)00057-6).
- [52] Praud F, Chatzigeorgiou G, Meraghni F. Fully integrated multi-scale modelling of damage and time-dependency in thermoplastic-based woven composites. *Int J Damage Mech* 2020;30:163–95. <https://doi.org/10.1177/1056789520944986>.
- [53] Sakai T, Hirai Y, Somiya S. Estimating the creep behavior of glass-fiber-reinforced polyamide considering the effects of crystallinity and fiber volume fraction. *Mech Adv Mater Mod Process* 2018;4. <https://doi.org/10.1186/S40759-018->

0038-4.

- [54] Chen Y, Huang S, Pickwell-MacPherson E, Ashworth PC, Pickwell-MacPherson E, Provenzano E, et al. Frequency-wavelet domain deconvolution for terahertz reflection imaging and spectroscopy. *Opt Express* 2010;18:1177–90. <https://doi.org/10.1364/OE.18.001177>.
- [55] Mittleman DM, Jacobsen RH, Neelamani R, Baraniuk RG, Nuss MC. Gas sensing using terahertz time-domain spectroscopy. *Appl Phys B Lasers Opt* 1998;67:379–90. <https://doi.org/10.1007/S003400050520>.
- [56] Potter K, Khan B, Wisnom M, Bell T, Stevens J. Variability, fibre waviness and misalignment in the determination of the properties of composite materials and structures. *Compos Part A Appl Sci Manuf* 2008;39:1343–54. <https://doi.org/10.1016/J.COMPOSITESA.2008.04.016>.